Gating Charge Immobilization in Kv4.2 Channels: The Basis of Closed-State Inactivation

Kevin Dougherty, Jose A. De Santiago-Castillo, and Manuel Covarrubias

Department of Pathology, Anatomy, and Cell Biology, Jefferson Medical College of Thomas Jefferson University, Philadelphia, PA 19107

Kv4 channels mediate the somatodendritic A-type K^+ current (I_{SA}) in neurons. The availability of functional Kv4 channels is dynamically regulated by the membrane potential such that subthreshold depolarizations render Kv4 channels unavailable. The underlying process involves inactivation from closed states along the main activation pathway. Although classical inactivation mechanisms such as N- and P/C-type inactivation have been excluded, a clear understanding of closed-state inactivation in Kv4 channels has remained elusive. This is in part due to the lack of crucial information about the interactions between gating charge (Q) movement, activation, and inactivation. To overcome this limitation, we engineered a charybdotoxin (CTX)-sensitive Kv4.2 channel, which enabled us to obtain the first measurements of Kv4.2 gating currents after blocking K^+ conduction with CTX (Dougherty and Covarrubias. 2006 *J. Gen. Physiol.* 128:745–753). Here, we exploited this approach further to investigate the mechanism that links closed-state inactivation to slow Q-immobilization in Kv4 channels. The main observations revealed profound Q-immobilization at steady-state over a range of hyperpolarized voltages (−110 to −75 mV). Depolarization in this range moves <5% of the observable Q associated with activation and is insufficient to open the channels significantly. The kinetics and voltage dependence of Q-immobilization and ionic current inactivation between −153 and −47 mV are similar and independent of the channel's proximal N-terminal region (residues 2–40). A coupled state diagram of closed-state inactivation with a quasi-absorbing inactivated state explained the results from ionic and gating current experiments globally. We conclude that Q-immobilization and closed-state inactivation at hyperpolarized voltages are two manifestations of the same process in Kv4.2 channels, and propose that inactivation in the absence of N- and P/C-type mechanisms involves desensitization to voltage resulting from a slow conformational change of the voltage sensors, which renders the channel's main activation gate reluctant to open.

INTRODUCTION

Members of the Kv4 subfamily of voltage-gated K^+ channels mediate the somatodendritic A-type K^+ currents (I_{SA}) in neurons (Serodio et al., 1994; Jerng et al., 2004; Birnbaum et al., 2004). Among many important roles, I_{SA} attenuates back-propagating action potentials, regulates the firing frequency, electrically sequesters dendrites from one another, and aids in action potential repolarization (Hoffman et al., 1997; Cai et al., 2004; Kim et al., 2005). Largely, I_{SA} performance depends on the availability of functional Kv4 channels, which is dynamically regulated by the membrane potential. Depolarized and hyperpolarized voltages decrease and increase channel availability, respectively. Presumably, subthreshold depolarizations trigger rearrangements within Kv4 channels that render them refractory to subsequent activation. These processes are generally referred to as inactivation, and may proceed via a variety of distinct mechanisms.

The mechanisms underlying Kv4 channel inactivation have not been resolved. A nonconventional form of N terminus–dependent (N-type) inactivation was demonstrated in Kv4.2 α subunits expressed alone (Gebauer et al., 2004). However, neuronal Kv4 channels are expressed as integral oligomeric complexes with auxiliary subunits including K^+ channel–interacting proteins (KChIPs), which bind and functionally sequester the Kv4 N-terminal inactivation domain (An et al., 2000; Beck et al., 2002; Pioletti et al., 2006; Wang et al., 2007a). Thus, many KChIPs preclude the N-type–like inactivation mechanism in vivo. An intriguing aspect of Kv4 channel inactivation is that it remains relatively rapid and complete when N-type–like inactivation is eliminated by an N-terminal deletion (Δ2–40 Kv4.2) or when the channels are coexpressed with KChIPs (Zhu et al., 1999; Bähring et al., 2001b; Beck et al., 2002; Kaulin et al., 2007). Collectively, electrophysiological observations under various conditions strongly suggest a prominent role of closed-state inactivation (CSI) in Kv4 channel gating: (a) voltage-dependent inactivation is rapid and

Correspondence to Manuel Covarrubias: Manuel.Covarrubias@jefferson.edu

The online version of this article contains supplemental material.

Abbreviations used in this paper: CSI, closed-state inactivation; CTX, charydbotoxin; HCN, hyperpolarization and cyclic nucleotide–regulated; I_{SS}, steady-state inactivation; KChIP, K^+ channel interacting protein.

J. Gen. Physiol. © The Rockefeller University Press $30.00
Volume 131 Number 3 March 2008 257–273
http://www.jgp.org/cgi/doi/10.1085/jgp.200709938

complete at relatively hyperpolarized voltages where the open probability is negligible; (b) macroscopic inactivation at progressively depolarized membrane potentials slows gradually as the open probability increases; (c) voltage-dependent recovery from inactivation does not require reopening and is typically complete in hundreds of milliseconds; (d) blank sweeps are commonly observed at the single channel level (Bähring et al., 2001a; Beck and Covarrubias, 2001; Beck et al., 2002). Physiologically, CSI would be an effective way to regulate the resting membrane potential–dependent availability of Kv4 channels in the nervous system. However, the events leading to CSI and its molecular basis remain poorly understood.

In general, CSI is more difficult to study than open-state inactivation because ionic currents only provide an indirect evaluation of this process. Measurements of gating charge (Q) movement are a more direct way to visualize transitions involving closed states in the main activation pathway of voltage-gated ion channels (Bezanilla, 2000). Previous studies have demonstrated that inactivation is associated with Q-immobilization in voltage-gated ion channels (Armstrong and Bezanilla, 1977; Bezanilla et al., 1982, 1991; Ruben et al., 1992; Fedida et al., 1996; Olcese et al., 1997; Roux et al., 1998; Sheets et al., 2000). The apparent immobilization is observed when some fraction of the gating current relaxes very slowly over an extended period of time; and, as a result, the corresponding Q is undetectable (an apparent Q loss). In Shaker-B and other Kv1 channels, there are two distinct forms of Q-immobilization: fast and slow. Fast Q-immobilization results from fast N-type inactivation, which slows the return of the Q upon repolarization (Q_{OFF}), and is therefore a byproduct of the open-channel blockage that underlies N-type inactivation (Bezanilla et al., 1991; Roux et al., 1998). Although the origin of slow Q-immobilization is less clear, solid evidence suggests a connection to slow P/C-type inactivation, which is associated with a localized collapse of the channel's selectivity filter (Yellen et al., 1994; Olcese et al., 1997; Cordero-Morales et al., 2007). In this case, fast voltage sensor movements responsible for activation trigger P/C-type inactivation, and slow Q-immobilization stabilizes the P/C-type inactivated state (Loots and Isacoff, 1998; Larsson and Elinder, 2000). Therefore, slow Q-immobilization in Shaker-B Kv channels is an accessory to inactivation. A simple extrapolation of the N-type and P/C-type mechanisms to Kv4 channels, however, is precluded because they do not exhibit the classical N-type (under physiological conditions; see above) and P/C-type mechanisms, which generally involve interrupting conduction of open channels.

Recently, we reported the first measurements of Kv4.2 gating currents by using a charybdotoxin (CTX)-based strategy to block ionic currents (Dougherty and Covarrubias, 2006). By extending the application of this strategy, the main thrust of the work reported here was to determine the probable correlation between Q-immobilization and CSI in Kv4 channels. Such a correlation in the absence of classical inactivation mechanisms would suggest that Q-immobilization and CSI in Kv4 channels are equivalent manifestations of a process that renders the channels reluctant to open and seemingly desensitized to voltage. In hyperpolarization-activated cyclic nucleotide–regulated cationic (HCN) channels, desensitization to voltage was proposed as a mechanism of CSI (Shin et al., 2004); however, whether desensitization to voltage in HCN channels involves a conformational change of the voltage sensor was not determined. We will discuss slow Q-immobilization in Kv4 channels as the mechanism that promotes desensitization to voltage and thereby causes CSI.

MATERIALS AND METHODS

Cell Culture and Channel Expression

Wild-type Kv4.2 cDNA (a gift from M. Sheng, Massachusetts Institute of Technology, Cambridge, MA) was maintained in pRc-cytomegalovirus (CMV; Invitrogen). Three mutations near the pore helix of Kv4.2 were necessary to confer CTX sensitivity (Kim et al., 2004; Dougherty and Covarrubias, 2006). The CTX-sensitive Kv4.2 mutant, which will, from this point onward, be referred to as Kv4.2, was created with the QuickChange site-directed mutagenesis kit (Stratagene) and confirmed by automated sequencing at the Nucleic Acid Facility of the Kimmel Cancer Center (Thomas Jefferson University). Δ2–40 Kv4.2 was subcloned into the pEGFP-N1 plasmid (CLONTECH Laboratories, Inc.), with a stop codon immediately following the Kv4.2 C terminus. Shaker-B Kv channels bearing the mutations W434F and T449V (a gift from R. Horn, Thomas Jefferson University) was maintained in the GWI-CMV vector (British Biotechnology); and was used as a "noninactivating" control because the T449V mutation impairs slow conformational changes associated with C-type inactivation (Olcese et al., 2001). The transfection of tsA-201 cells (a gift from R. Horn) was accomplished by the calcium-phosphate method (O'Leary and Horn, 1994), and a plasmid containing the CD8 gene was cotransfected to allow the identification of individual transfected cells by labeling them with beads bearing anti-CD8 antibody (Dynal) (Jurman et al., 1994). Recombinant CTX (98% pure) was purchased from Sigma-Aldrich.

Electrophysiology

Ionic currents were measured in the tight-seal whole-cell configuration of the patch-clamp method with the following pipette (intracellular) solution (in mM): 120 KF, 1 $CaCl_2$, 2 $MgCl_2$, 11 EGTA, and 10 HEPES, pH 7.2, adjusted with KOH; and the following external bath solution (in mM): 150 NaCl, 2 KCl, 1.5 $CaCl_2$, 1 $MgCl_2$, and 10 HEPES, pH 7.4, adjusted with NaOH. Series resistances (2–5 MΩ) were compensated to yield a total voltage error of ≤3 mV. Gating currents (I_g) were measured with the following pipette (intracellular) solution (in mM): 105 CsF (replaced with 105 NMG-F in Fig. S1, available at http://www.jgp.org/cgi/content/full/jgp.200709938/DC1), 35 NaCl, 10 EGTA, and 10 HEPES, pH 7.4, adjusted with CsOH; and the following external solution (in mM): 135 NMG-Cl, 2 KCl, 10 HEPES, 1 $MgCl_2$, and 1 $CaCl_2$, pH 7.4, adjusted with HCl. Unless otherwise indicated, all Kv4.2 I_gs were recorded in the presence of ∼100 nM CTX. I_gs from Shaker Kv channels (W434F - T449V) were recorded with the Cs^+-containing pipette solution and the Na^+-containing bath

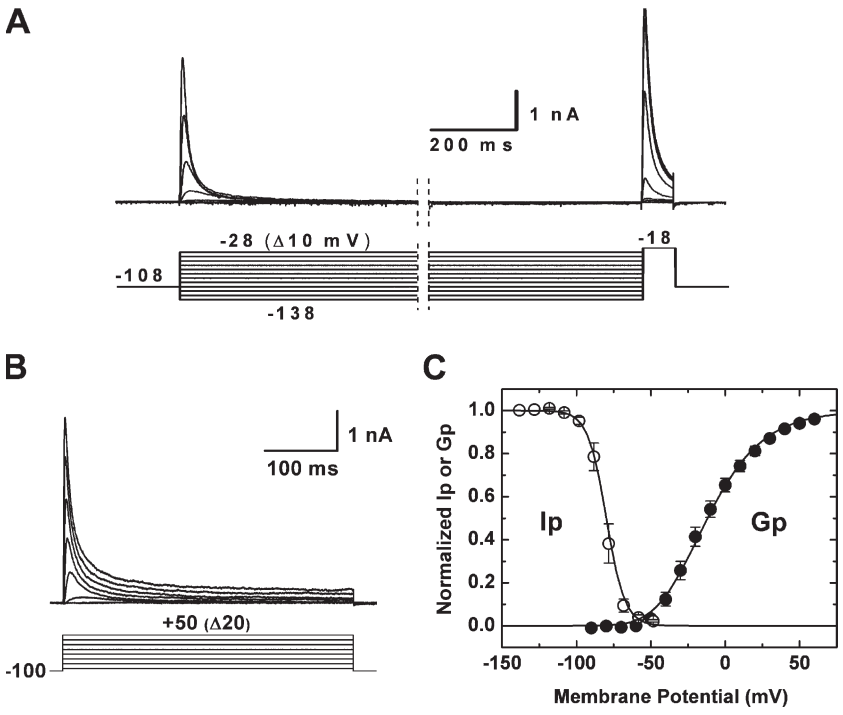

Figure 1. Non-overlapping voltage dependencies of steady-state inactivation and peak conductance. (A) Steady-state inactivation was induced in Kv4.2 channels by 10-s voltage steps between −138 to −28 mV from a holding potential of −108 mV followed by a test pulse to −18 mV. (B) Macroscopic currents were elicited by 400-ms step depolarizations ranging from −90 to +50 mV from a holding potential of −100 mV. (C) Steady-state inactivation and peak conductance occur in separate voltage ranges. Steady-state inactivation (hollow circles) was described by assuming a Boltzmann function with $V_{1/2} = -81$ mV and $k = 5.7$ mV. Peak G-V (Gp-V; filled circles) curve was described assuming a fourth-order Boltzmann function with $V_{1/2} = -13.4$ mV and $k = 23.2$ mV. The number of independent experiments is indicated in Table I.

solution described above. Simultaneous immobilization-inactivation experiments (Figs. 8 and 9) were conducted with the following pipette (internal) solution (in mM): 3.8 CsCl, 101 NMG-F, 35 NaCl, 10 EGTA, and 10 HEPES, pH 7.4 adjusted with HF; and the following external (bath) solution (in mM): 15 CsCl, 137 NMG-Cl, 1.5 $CaCl_2$, 1 $MgCl_2$ 10 HEPES, pH 7.4 adjusted with HCl. The calculated Cs^+ reversal potential was +35 mV. To subtract passive components of the total current and isolate the I_g, a P/−4 leak subtraction protocol was applied before the test pulses. It consisted of four subpulses from a subsweep holding potential of −153 mV. All I_g measurements were filtered at 5 kHz and sampled at 25 kHz. Analyses and graphical displays were produced with pClamp (versions 9.0 and 10.0; Molecular Devices) and Origin (version 7.5; OriginLab) software. The calculated liquid junction potential was subtracted off-line. All measurements were taken at room temperature (22–25°C).

Data Analysis

Q_{ON} and Q_{OFF} values were obtained by integrating the area under the gating current trace for the length of the entire depolarization and repolarization, respectively. Normalized Q-V, Q-availability, and steady-state inactivation (Iss) curves were empirically described by assuming a Boltzmann function: $y(V) = 1/1 + \exp((V - V_{1/2})/k))$, while Gp-V relations were described by assuming a Boltzmann function raised to the fourth power (Zagotta et al., 1994b); $y(V)$ is the voltage-dependent variable, k is the slope factor, and $V_{1/2}$ is the midpoint voltage. At hyperpolarized and modestly depolarized membrane potentials, single exponential relaxations were sufficient to describe the development of inactivation and Q-immobilization and the corresponding time courses of recovery. The bell-shaped voltage dependence of the time constants of inactivation and Q-immobilization were described empirically by assuming the following equation: $\tau(V) = 1/(A_0\exp(z_A e_{0A} V/k_b T) + B_0\exp(-z_B e_{0B} V/k_b T)) + C$, where A_0 and B_0 represent the rate constant at 0 mV, z_A and z_B represent the equivalent valence, and e_{0A} and e_{0B} represent the electronic charge; $k_b T$ has its typical thermodynamic meaning. All data are expressed as mean ± SEM, and a one-way ANOVA test was used to evaluate differences.

Global Kinetic Modeling

To explain the experimental observations from ionic and gating currents more quantitatively, we developed a robust global kinetic modeling approach. It aims at determining a physiologically plausible Markov state diagram that simultaneously describes the time and voltage-dependent macroscopic properties of ionic and gating currents. The program IChMASCOT (Ion Channel Markov Scheme Optimizer) was used to evaluate and generate the global fits (www.ichmascot.org). Here, the model was constrained simultaneously by several macroscopic measurements over a 250-mV range of membrane potentials, which included the development of activation, inactivation, deactivation, recovery form inactivation (Fig. 13, A–C) and gating currents (Fig. 13 D). Also, the steady-state inactivation curve (Fig. 14 B) and the voltage dependence of the time constants of inactivation were included in the global dataset (Fig. 14 C); and the total number of channel was assumed to be constant. In IChMASCOT, the rate constants and associated apparent charges of the transitions in a kinetic model are obtained from the best-fit parameters resulting from minimization of the squared differences between the observed and the modeled values according to:

$$d = \sum_{i=1}^{N} W_i \sum_{j=1}^{M_i} (E_{ij} - S_{ij})^2, \text{ with } W_i = \frac{w_i}{M_i {E_{i_{\max}}}^2},$$

where N is the number of different measurements (e.g., activation, deactivation, etc); M_i is the number of independent experimental observations in the dataset i; E_{ij} and S_{ij} are the experimental observations and corresponding modeled values, respectively; w_i is an arbitrary weight factor for the measurement i; W_i is the normalized weight factor for specific dataset; and E_{imax} is the maximal experimental value for the dataset i. The weight factor W_i is necessary to correct for large numerical differences in the absolute values of the observations (e.g., activation and time constant–voltage relation), which otherwise would result in unreliable modeling results. The program IChSimLab (Ion Channel Simulation Laboratory; www.ichmascot.org) was used to produce the model simulations.

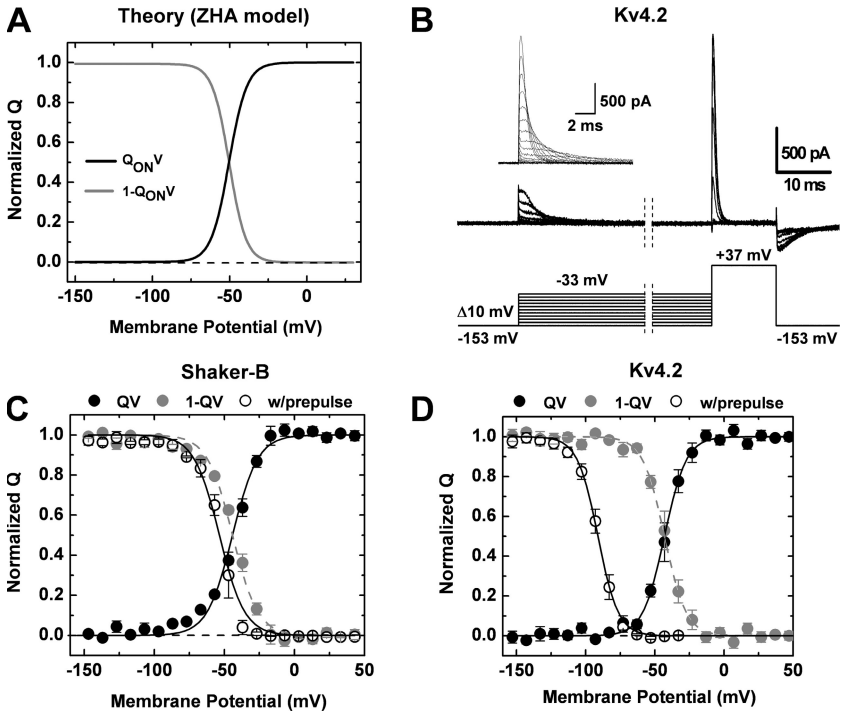

Figure 2. Q-immobilization at hyperpolarized potentials. (A) Simulation assuming an "inactivation-less" Kv channel (based on the ZHA model for Δ6–46 Shaker-B channels; see text) predicts that the $Q_{ON}V$ (black line) and available 1 − $Q_{ON}V$ (gray line) curves cross at their midpoints. (B) Available Q (hollow circles in C and D) was assayed in Kv4.2 channels by a step depolarization to +37 mV after a 900-ms prepulse between −153 and −33 mV in 10-mV increments from a holding potential of −153 mV. Inset, Kv4.2 gating currents elicited by 12-ms step depolarizations between −143 and +37 mV in 10-mV increments from a holding potential of −153 mV. (C) The above protocol was applied to mutant Shaker-B channels (W434F-T449V). For comparison, the $Q_{ON}V$, 1 − $Q_{ON}V$, and the Q-availability curves are shown superimposed. Data were described by assuming a Boltzmann function with the following best-fit parameters for the $Q_{ON}V$ curve: $V_{1/2}$ = −44.2 mV, z = 2.8 e_0; and the Q-availability curve: $V_{1/2}$ = −53.6 mV, z = 2.8 e_0, n = 4. (D) QV curves from Kv4.2 channels were described by Boltzmann functions assuming the following parameters for the $Q_{ON}V$: $V_{1/2}$ = −43.0 mV, z = 3.4 e_0; and the Q-availability curve: $V_{1/2}$ = −91.2 mV, z = 3.5 e_0, n = 7. The ΔV between these curves is 48 mV.

Online Supplemental Material

The online supplemental material (available at http://www.jgp.org/cgi/content/full/jgp.200709938/DC1) includes a summary of the theory applied to conduct the kinetic simulations and the installation and documentation files for the computer program IChSim. Also, it includes the following supplemental data: Fig. S1 shows that intracellular Cs^+ does not significantly affect the kinetics of Q-immobilization; Fig. S2 is an alternate depiction of the proposed kinetic scheme, which is used for proper identification of individual states; Fig. S3 demonstrates Monte Carlo simulations illustrating the voltage dependence of the kinetics of closed-state inactivation at the single channel level; and Fig. S4 compares the observed family of Kv4.2 gating currents and the corresponding best-global-fit (without consideration of ionic current parameters).

RESULTS

Inactivation and Q-immobilization in Kv4.2 Channels at Hyperpolarized Voltages

Profound prepulse inactivation over a relatively narrow range of hyperpolarized voltages is a hallmark of Kv4 channels. Fig. 1 illustrates this feature for Kv4.2 channels expressed in tsA-201 cells. To ensure steady state, the duration of the conditioning prepulses in these experiments was 10 s. The resulting voltage dependence of steady-state inactivation was well described by assuming a Boltzmann distribution with the following midpoint

TABLE I

Gating Parameters of Kv4.2 Channels

	Kv4.2 WT	Kv4.2 CTX-sensitive mutant	Δ2–40 Kv4.2 CTX-sensitive mutant
Gp-V: $V_{1/2}$ (mV)	−6.6 ± 1.5 (4)[a]	−13.4 ± 2.9[b] (7)	−22.1 ± 2.0[b] (4)
k (mV)	26.7 ± 1.1 (4)[a]	22.4 ± 1.1 (7)	23.1 ± 1.5 (4)
I_{SS}: $V_{1/2}$ (mV)	−77.4 ± 1.4[b] (5)	−80.1 ± 2.2 (5)	−84.0 ± 1.0[b] (4)
k (mV)	4.0 ± 0.2 (5)	4.5 ± 0.2 (5)	4.6 ± 0.3 (4)
$Q_{ON}V$: $V_{1/2}$ (mV)		−40.4 ± 2.2 (6)	−37.3 ± 2.2 (8)
z (e_0)		3.1 ± 0.3 (6)	3.6 ± 0.2 (8)
Q availability: $V_{1/2}$ (mV)	−50.1 ± 2.5 (3)[c]	−55.6 ± 3.4 (3)[c]	
z (e_0)	2.2 ± 0.2 (3)	1.7 ± 0.2 (3)	

The number of independent experiments is indicated in parentheses.
[a]Data taken from Table I of Dougherty and Covarrubias, 2006.
[b]Differences between the mean values are statistically significant at the $P < 0.05$ level in a one-way ANOVA test. Differences between the means of all other parameters are not statistically significant at $P < 0.05$.
[c]From experiments shown in Fig. 9 C.

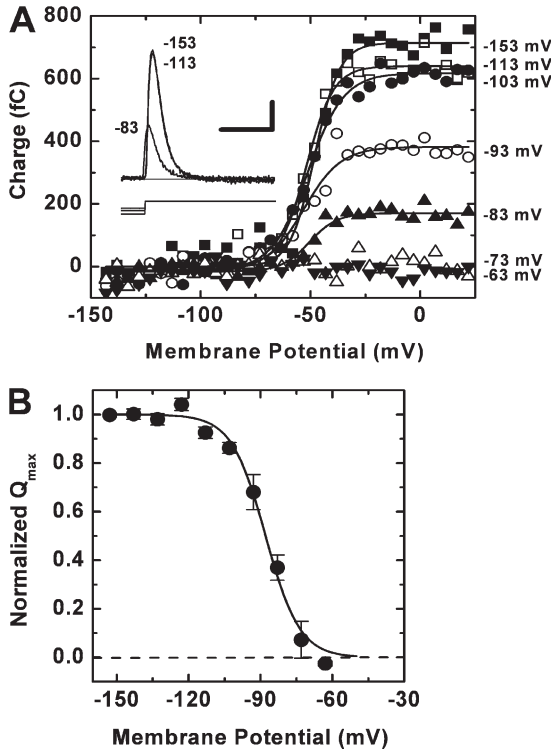

Figure 3. Holding potential dependence of Q availability. (A) $Q_{ON}V$ curves were generated between −143 and +22 mV in 5-mV increments from the indicated holding potentials, and the start-to-start interval was 7 s. Each curve was described by assuming a Boltzmann function to estimate the maximal Q ($Q_{ON\text{-}MAX}$). Inset, gating currents were elicited by step depolarizations to +2 mV from the indicated holding potentials. The scale bars correspond to 5 ms and 500 pA. (B) The holding potential dependence of normalized $Q_{ON\text{-}MAX}$ was described by assuming a Boltzmann function with the following best-fit parameters: $V_{1/2}$ = −88 mV and z = 3.6 e_0; n = 3–7 independent determinations.

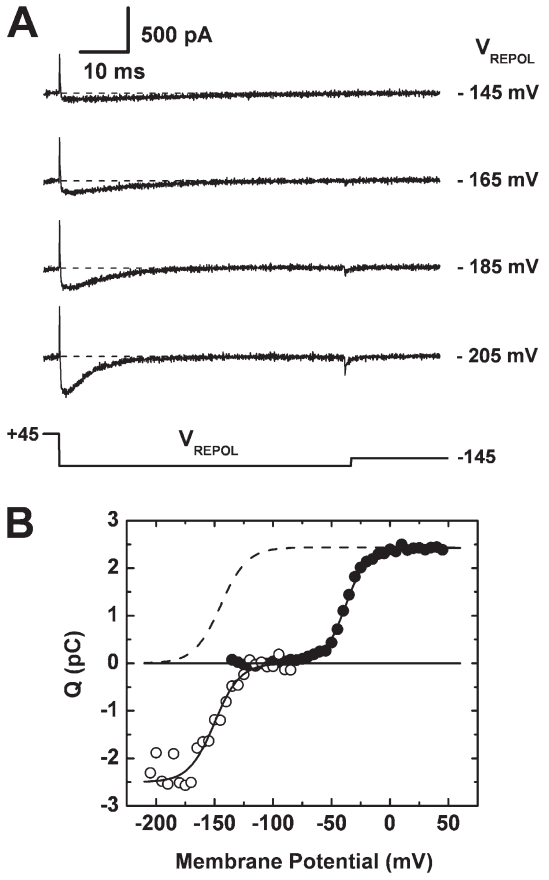

Figure 4. Q of Kv4.2 channels can move in two energetically distinct pathways. (A) OFF gating currents after a sustained depolarization. From a holding potential of +45 mV, the immobilized Q was "reclaimed" by 60-ms step repolarizations between −205 and −85 mV in 5-mV increments. Initially, membrane potential was held at +45 mV for over 1 min, and for over 7 s between sweeps. The apparent downward deflection elicited by the step from V_{REPOL} to −145 mV is a small unsubtracted nonlinear component of the capacitive current. We expect no Q movement in this range of membrane potentials (Fig. 2 D). (B) The $Q_{ON}V$ curve from a holding potential of −145 mV (filled circles) was described assuming a Boltzmann function (solid black line) with $V_{1/2}$ = −38 mV and z = 3 e_0, while the QV curve from a holding potential of +45 mV (hollow circles) was described assuming a Boltzmann function (solid gray line) with $V_{1/2}$ = −149 mV and z = 2.3 e_0. For comparison, the dashed line represents the transposed gray curve. The maximal and minimal absolute Q values are ∼2.5 pC, indicating that Q is conserved (i.e., no loss of channels). The midpoints of the two QV curves are separated by ∼110 mV. The same result was obtained in an independent repetition of this experiment.

voltage and slope factor: −81 mV and 5.7 mV, respectively (Table I). Also, it is apparent that the fraction of available channels decreases 90% between −100 and −70 mV; and within this voltage range there is no detectable activation of the conductance (Fig. 1 C). Moreover, as is characteristic of Kv4 channels, the currents inactivate rapidly and fully at negative voltages (Fig. 1 A and Fig. 5 A) and more slowly or incompletely at positive voltages where the open probability increases gradually near the plateau of the Gp-V curve (Fig. 1, B and C) (Jerng et al., 2004; Kaulin et al., 2007). These observations are consistent with the concept of closed-state inactivation as the mechanism that regulates the availability of functional Kv4.2 channels. The strong voltage dependence of steady-state inactivation indicates interactions involving the channel's voltage-sensing apparatus. Thus, we investigated Q-immobilization associated with inactivation at hyperpolarized voltages.

We hypothesized that Kv4.2 closed-state inactivation can induce an apparent loss of the available Q. This hypothesis is based on the strict quantitative relationship between the Q moved upon voltage-dependent activation ($Q_{ON}V$ curve) and the available Q (1 − $Q_{ON}V$ curve). Fig. 2 A illustrates this relationship for a hypothetical "inactivation-less" Kv channel and demonstrates that the $Q_{ON}V$ and 1 − $Q_{ON}V$ curves are exact mirror images, which cross at the midpoint voltage. That is, the Q that moves at a given voltage is equal to the Q that is no longer available at that voltage (i.e., Q is conserved). However, if apparent Q-immobilization occurs as a result of inactivation, prolonged depolarizations should

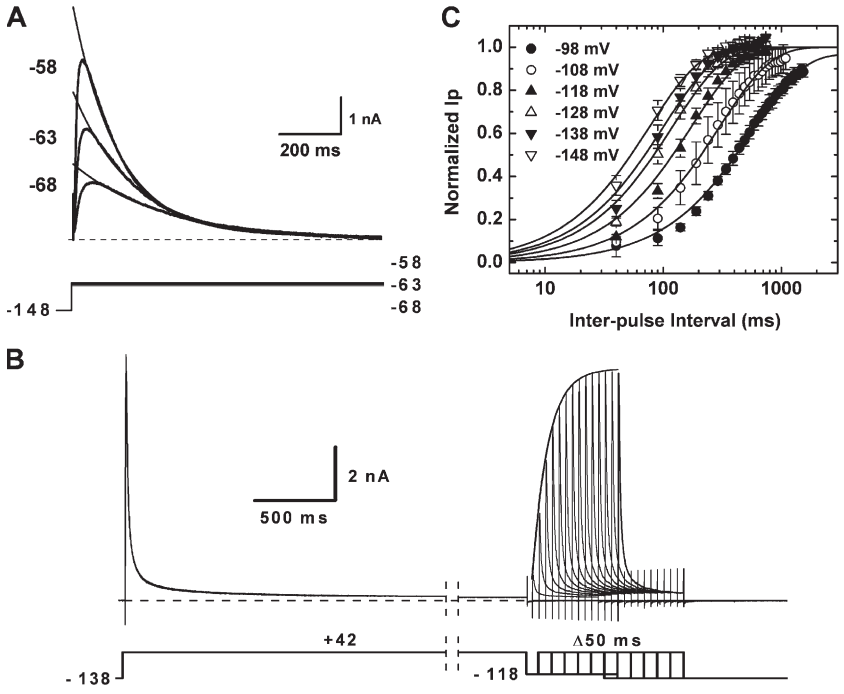

Figure 5. Kinetics of current inactivation in Kv4.2 channels. (A) Macroscopic K^+ currents were elicited by step depolarizations between −68 and −58 mV from a holding potential of −148 mV. Macroscopic inactivation at low P_o was described by assuming an exponential relaxation (black lines). (B) Kv4.2 channels were inactivated by a 10-s depolarization to +42 mV from a holding potential of −138 mV, and then allowed to recover for a variable duration at −118 mV before a test pulse to +42 mV. The black line superimposed on the recovery time course represents the best exponential fit. (C) Normalized recovery time courses were described by assuming exponential time dependence at the indicated recovery voltages; n = 3–5 independent experiments.

induce a hyperpolarizing shift of the $1 - Q_{ON}V$ curve, which breaks the strict relationship described above. In this case, the available Q is less than expected at a given voltage. To test these predictions, the $Q_{ON}V$ and calculated $1 - Q_{ON}V$ curves of Shaker-B (W434F-T449V) and Kv4.2 channels were compared with the observed Q-availability curves determined after 900-ms prepulses over a range of voltages (−153 to −33 mV; Fig. 2, B-D). The Shaker-B mutant channels exhibited little or no inactivation in this voltage range; therefore, in the examined time frame, the Q-availability curve was only slightly shifted to the left by <10 mV with respect to the calculated $1 - Q_{ON}V$ curve (Fig. 2 C). In contrast and under identical experimental conditions, the Q-availability curve of Kv4.2 channels was leftward shifted by 51 mV (Fig. 2 D). This observation indicates that the apparent loss of Q may result from inactivation induced by the 900-ms prepulses. It is also striking that the Q-availability curve falls sharply with a midpoint voltage at −91 mV (Table I) and that Q-immobilization is nearly complete (∼99%) at voltages that move ≤10% of the observable Q associated with voltage-dependent activation (Fig. 1 D).

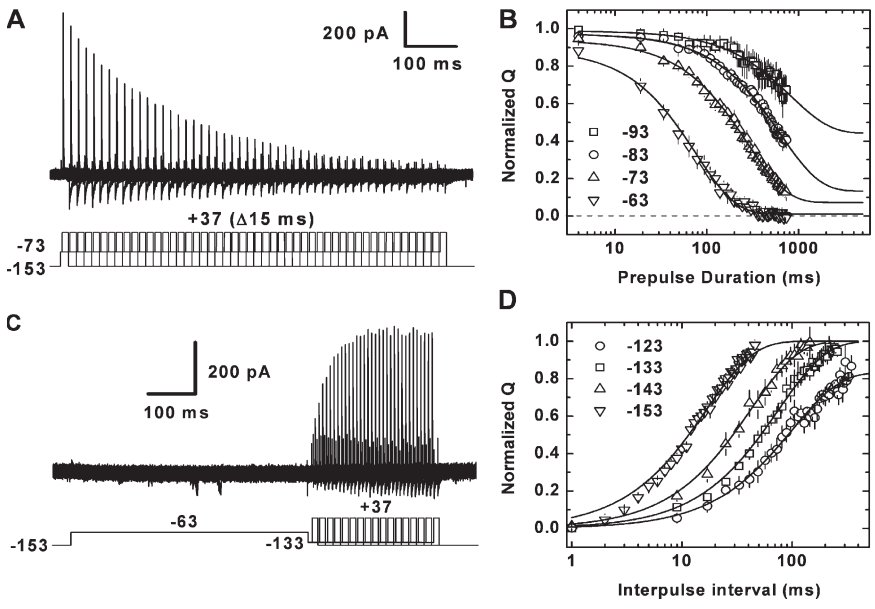

Figure 6. Kinetics of Q-immobilization in Kv4.2 channels. (A) Gating currents were elicited by step depolarizations to +37 mV following a prepulse of variable duration to −73 mV from a holding potential of −153 mV. (B) The time course of Q-immobilization was described by assuming exponential time dependence at the indicated prepulse voltages. The top of the curves is <1 at membrane potentials greater than −75 mV because an appreciable amount of Q associated with activation has moved (Figs. 8 and 9); n = 3–6 independent experiments. (C) Q-immobilization was installed by a 500-ms pulse to −63 mV, which is sufficient to establish steady state. Recovery from Q-immobilization (remobilization) was assayed by a step depolarization to +37 mV after a variable recovery interval at −133 mV. (D) Recovery from Q-immobilization was described by assuming exponential time dependence at the indicated recovery voltages; n = 3–5 independent experiments.

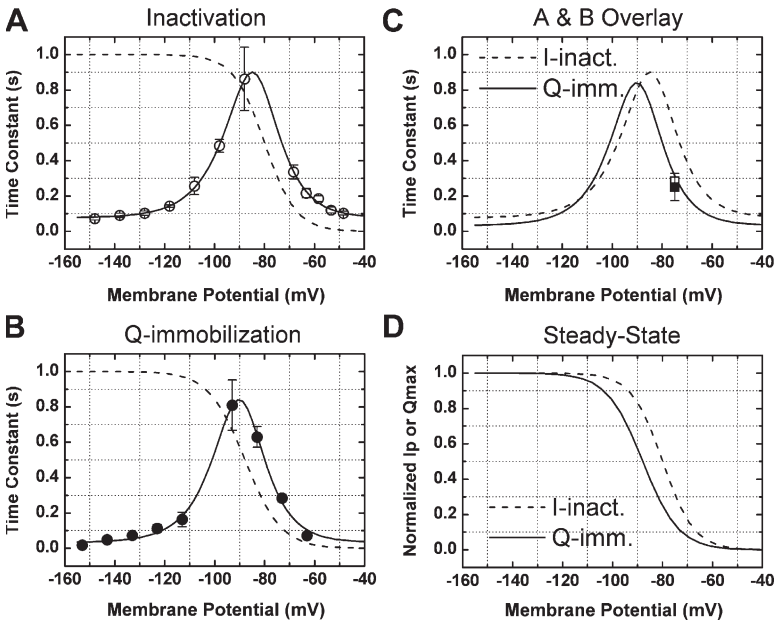

Figure 7. Voltage dependence of the time constants of inactivation and Q-immobilization. (A) Time constants of recovery from inactivation and macroscopic inactivation at low P_o (Fig. 5) against membrane potential (hollow circles) and the scaled I_{SS} curve from Fig. 1 C (dashed line). (B) Time constants of the development of Q-immobilization and the corresponding recovery process (Fig. 6) against membrane potential (filled circles) and the scaled steady-state Q-availability curve from Fig. 3 B (dashed line). Voltage dependence of the time constants in A and B were described as explained under Materials and methods (Data Analysis). The peaks of the resulting bell-shaped curves (solid lines) correspond with the midpoint of the steady-state curves (dashed lines). (C) For comparison, fitted curves from A (dashed line) and B (solid line) were superimposed. Squares represent the time constants of inactivation from measurements in Figs. 8 and 9, which report current inactivation in the presence of Cs^+ as the permeant ion. Filled and hollow squares correspond to wild-type Kv4.2 and CTX-sensitive Kv4.2, respectively. Note that when the ionic conditions of the measurements are similar (Cs^+ instead of K^+) there is a close agreement between the time constants of inactivation and Q-immobilization. (D) Boltzmann curves representing the I_{SS} (dashed line) and steady-state Q availability (solid line).

To confirm Q-immobilization at steady state, we investigated the holding potential dependence of the maximal Q ($Q_{ON\text{-}MAX}$, the plateau level of the $Q_{ON}V$ curve) (Fig. 3). When the holding potential was between −153 and −120 mV, $Q_{ON\text{-}MAX}$ remained constant; but as the holding potential became more depolarized, $Q_{ON\text{-}MAX}$ decreased gradually over a relatively narrow range of voltages (−113 to −73 mV; Fig. 3, A–C). Assuming a Boltzmann distribution, the midpoint voltage and apparent charge of this relationship were −88 mV and 3.6 e_0, respectively. Altogether, these results suggest that Kv4.2 inactivation at hyperpolarized membrane potentials is associated with an apparent Q loss. Also, the absence of a significant overlap between the $Q_{ON}V$ and Q availability curves (Fig. 2 D) is consistent with the presence of closed-state inactivation in Kv4.2 channels.

Previous studies reported leftward shifted $Q_{ON}V$ curves of inactivated Na^+ and Shaker channels and suggested that the Q movements from inactivated and noninactivated channels do not follow the same kinetic pathways (Bezanilla et al., 1982; Ruben et al., 1992; Olcese et al., 1997). To ask whether the Q of Kv4.2 channels can also move along two separate kinetic pathways, we investigated the movement of the Q after achieving complete steady-state inactivation at +45 mV (Fig. 4). Q movement was clearly apparent as the membrane potential is hyperpolarized between −175 and −200 mV, and the total expected Q was reclaimed fully as the repolarization reached −200 mV (Fig. 4 B). Furthermore, the corresponding QV curve exhibited an apparent hyperpolarizing shift of about ∼100 mV when compared with the QV curve resulting from gating currents evoked from a holding potential of −145 mV (Fig. 4 B). This result demonstrates, as shown for Shaker-B Kv channels (Olcese et al., 1997), that the voltage sensors of steady-state–inactivated Kv4.2 channels also see a distinct energetic landscape. However, the magnitude of the leftward shift in Kv4.2 channels is exaggerated because Q movement is very slow upon repolarization from +45 mV to negative membrane potentials (−135 to −165 mV; e.g., first two traces in Fig. 4 A) and, therefore, Q detection is incomplete. Q recovery experiments demonstrated that the total Q returns in ∼100 ms at −153 mV (Fig. 6 B). Therefore, a relatively small and slow Q movement resulting from repolarization of the membrane potential cannot be fully detected under experimental conditions. This limitation causes an apparently incomplete Q movement when repolarizing from +45 mV to voltages ranging between −160 and −140 mV (Fig. 4). However, if the total Q were somehow detected in this experiment, the Q observed between −200 and −125 mV would be identical. That is, we do not expect voltage-dependent Q movement in this range as confirmed in Fig. 2 D (hollow symbols) and Fig. 3 B, which show that the available Q at steady state does not begin to move significantly until the membrane potential reaches −113 mV.

Kinetics of Inactivation and Q-immobilization in Kv4.2 Channels

So far, we have established the presence of Q-immobilization associated with steady-state inactivation in Kv4.2 channels at hyperpolarized voltages. If Q-immobilization

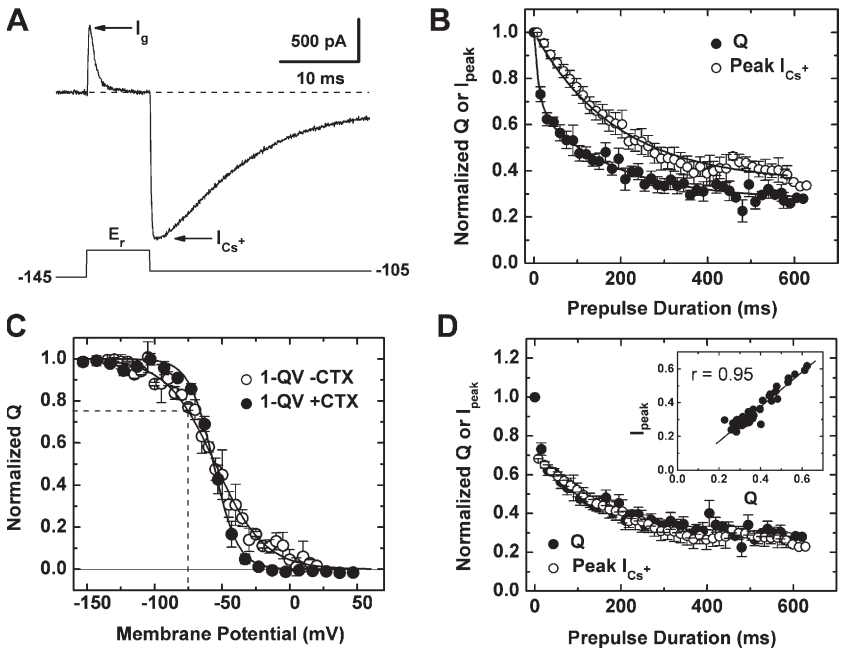

Figure 8. Simultaneous measurements inactivation and Q-immobilization. (A) Simultaneous measurement of gating and ionic currents was accomplished by a step depolarization to the Cs^+ reversal potential (Er = +35 mV; Materials and methods) to isolate the gating current and a subsequent hyperpolarization to −105 mV to evoke a Cs^+ tail current. Gating charge immobilization was assayed as the fraction of total charge remaining after a prepulse of variable duration to −75 mV, while inactivation was assayed by the fraction of tail current remaining in the same trace. The dashed line indicates the zero current level. (B) Gating charge immobilization (filled circles) was described assuming a bi-exponential function with the following best-fit parameters: τ_{fast} = 10.8 ms, relative weight = 0.31; τ_{slow} = 190 ms, relative weight = 0.43; and the relative weight of nonimmobilized Q = 0.25. Inactivation (hollow circles) was described by assuming an exponential function with the following best-fit parameters: τ = 228 ms, relative weight = 0.75; relative weight of noninactivated current = 0.25. The fast phase of the Q decay accounted for ∼30% of the total; n = 4. (C) Q availability curves following a 12-ms prepulse between −153 and + 47 mV for Kv4.2 channels in the presence (filled circles) and absence of CTX (hollow circles). These curves were described by assuming Boltzmann functions with the following best-fit parameters: $V_{1/2}$ (+CTX) = −53.2 mV, z (+CTX) = 2.9 e_0; $V_{1/2}$ (−CTX) = −54.8, z (−CTX) = 1.5 e_0. The dashed lines indicate that ∼25% of Q has been moved at −75 mV for Kv4.2 channels in the absence of CTX. (D) Inactivation was renormalized in order to facilitate comparison with the slow component of Q decay, yielding a compelling correlation between Q-immobilization and inactivation at −75 mV. Inset, correlation between $I_{PEAK\text{-}Cs^+}$ and Q; slope = 1.03 (r = 0.95).

and inactivation are indeed correlated, then they should share the same voltage-dependent kinetics. To test this hypothesis, we examined the development and recovery processes at voltages below and above the midpoints of steady-state inactivation and Q availability (Figs. 5–7). The development of inactivation was evaluated from the decays of the macroscopic currents evoked by step depolarizations ranging between −68 and −48 mV (5-mV intervals; Fig. 5 A). These measurements were possible because tsA-201 cells overexpress the recombinant Kv4.2 channel, which allowed detection of low open probability activity at negative voltages; and the development of inactivation was well approximated as an exponential process (Fig. 5 A). Recovery from inactivation was measured by applying a standard two-pulse protocol with a variable recovery interval at various hyperpolarized voltages ranging between −88 and −153 mV (10-mV intervals) (Fig. 5 B); and the recovery time course was also well described by assuming exponential kinetics (Fig. 5 C). The development of Q-immobilization was measured by progressively increasing the duration and voltage of a conditioning prepulse (−63 to −93 mV; 10-mV interval) and the available Q was evaluated by a test pulse to +37 mV (Fig. 6 A); and the recovery from Q-immobilization (remobilization) was measured at potentials ranging from −103 to −153 mV by applying a modified two-pulse protocol (Fig. 6 C, legend). The developments of Q-immobilization and remobilization were described by assuming exponential decays (Fig. 6, B and D). Plots of the voltage dependence of all time constants exhibited characteristic biphasic profiles, which were well described by assuming a bell-shaped logistic function (Fig. 7, A, B, and legend; Materials and methods). Significantly, the slowest points of the bell-shaped profiles (peak) correspond closely to the midpoint voltages of the inactivation and Q-immobilization curves at steady state, and both processes appeared associated with nearly identical apparent valences (Fig. 7, A and B). Thus, the datasets are internally consistent and assuming first-order equilibrium between closed and inactivated or immobilized channels is a reasonable initial approximation to characterize the observations. Suggesting a correlation and possible tight coupling between inactivation and Q-immobilization, a direct comparison of the two profiles revealed a significant similarity between the voltage dependencies of the time constants of both processes (Fig. 7 C). However, a differential shift between the two curves also suggested that the conditions necessary to measure gating currents (e.g., CTX and the absence of intracellular K^+; Materials and methods) may have introduced a slight voltage-dependent offset (ΔV = 8 mV) in the experiments (Fig. 7, C and D). Investigating the mechanism of this shift was, however, outside the scope of this study. Nevertheless, to probe the relationship between Q-immobilization and inactivation under more stringent conditions, both ionic and gating currents were measured simultaneously.

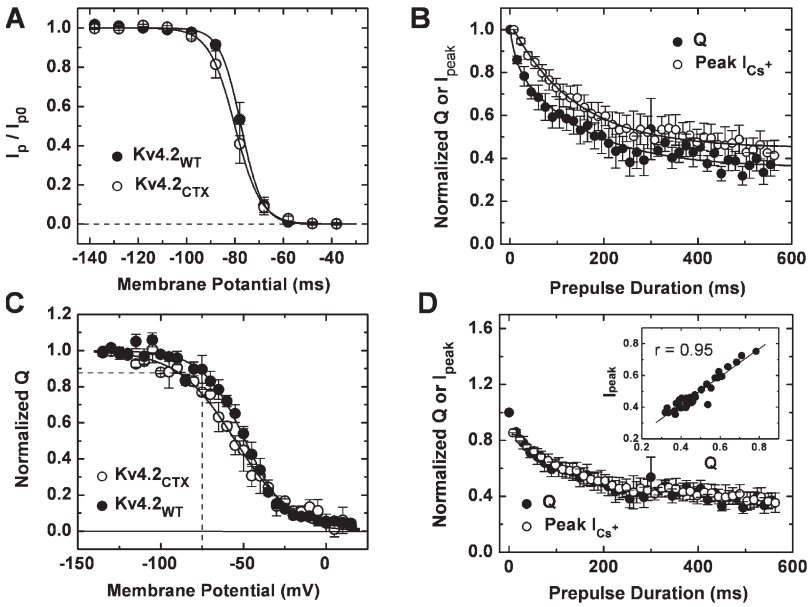

Figure 9. Simultaneous measurements of inactivation and Q-immobilization in wild-type Kv4.2 channels. (A) I_{SS} curves from CTX-sensitive Kv4.2 ($Kv4.2_{CTX}$, hollow circles) and wild-type Kv4.2 ($Kv4.2_{WT}$, filled circles) were described by assuming a Boltzmann function with the following best-fit parameters: $V_{1/2}$ ($Kv4.2_{WT}$) = −77.4 mV, k ($Kv4.2_{WT}$) = 4.4 mV; $V_{1/2}$ ($Kv4.2_{CTX}$) = −81 mV, k ($Kv4.2_{CTX}$) = 5.7 mV; n = 3. (B) Inactivation and Q-immobilization were measured simultaneously as explained in Fig. 8 legend. Data were described by assuming exponential time dependence with the following best-fit parameters: τ_{fast} (Q) = 15.9 ms, relative weight (Q) = 0.14, τ_{slow} (Q) = 146.5 ms, relative weight (Q) = 0.48, and relative weight of nonimmobilized Q = 0.37; τ (I_{Cs}^+) = 144.1 ms, relative weight ($I\,I_{Cs}^+$) = 0.58, weight of noninactivated current ($I\,I_{Cs}^+$) = 0.44; n = 3. (C) Q availability curves from $Kv4.2_{WT}$ channels were described by assuming a Boltzmann function with $V_{1/2}$ = −49 mV and z = 2 e_0; n = 3. Interpolation (dashed lines) indicates that ~15% of Q has moved at −75 mV in the absence of CTX. (D) Simultaneous inactivation and Q-immobilization measurements from B were renormalized as explained in Fig. 8 legend, which yielded a compelling correlation between inactivation and Q-immobilization. Inset, slope = 0.9 (r = 0.95).

Precise Temporal Equivalence of Inactivation and Q-immobilization in Kv4.2 Channels

Simultaneous measurements of Q-immobilization and inactivation were accomplished by replacing all permeant ions with Cs^+, and setting the Cs^+ current reversal potential (E_r) to +35 mV. These experiments were performed in the absence of CTX; and gating currents were then isolated from ionic currents by depolarization to Er, while Cs^+ tail currents were elicited by subsequent hyperpolarizations to −105 mV (Fig. 8 A). Q-immobilization and closed-state inactivation were induced by a conditioning prepulse of variable duration to −75 mV (the voltage at which the apparent offset was the largest; Fig. 7 C). Q-immobilization was gauged by the loss of available Q at Er, while inactivation was monitored by the reduction in the peak Cs^+ tail current. While the development of Cs^+ current inactivation was well described by assuming an exponential decay (τ = 227 ms), that of Q-immobilization required the sum of two exponential terms. This biexponential decay describes two distinct processes: the fast phase representing ~30% of the decay (τ_F = 10 ms) corresponds to Q movement associated with voltage-dependent activation; and the slow phase (τ_S = 190 ms) more likely corresponds to the slow Q movement associated with Q-immobilization. To verify the origin and amplitude of the fast phase, we constructed the $1 - Q_{ON}V$ curve under conditions identical to those of these experiments (i.e., no CTX) and determined that the fraction of Q movement associated with activation at −75 mV is ~25%, which is in excellent agreement with the kinetic measurement (Fig. 8 C). However, this estimate is modestly larger than the fraction measured in the presence of CTX (~10%) because the $1 - Q_{ON}V$ curve obtained in the absence of CTX was slightly shallower (Fig. 8 C). In light of these observations, a direct comparison of the kinetics of Cs^+ current inactivation and Q-immobilization was achieved by precisely shifting down the development of inactivation by 30% along the y axis (Fig. 8 D). The two time courses exhibited striking similarity and nearly exact correlation, which constitutes compelling evidence of a tight link between closed-state inactivation and Q-immobilization in Kv4.2 channels.

To rule out possible contributions of the three nonconservative CTX-sensitizing pore mutations to the observed correlations, the simultaneous measurements of ionic and gating currents were repeated with wild-type Kv4.2 channels. However, significant differences were not expected because the steady-state inactivation and the $1 - Q_{ON}V$ curves of wild-type and mutant channels were nearly identical (Fig. 9, A and C). Q-immobilization at −75 mV was again well described by the sum of two exponential terms, while an exponential decay was sufficient to describe inactivation (Fig. 9 B). The fast phase accounted for ~15% of the total Q decay, and the $1 - Q_{ON}V$ curve from wild-type Kv4.2 channels adequately verified the amplitude of the Q movement associated with activation at −75 mV (Fig. 9 C, dashed line). Thus, after proper adjustment (see above), the slow phase of Q-immobilization was precisely correlated with inactivation, confirming that the two processes are also tightly linked in wild-type Kv4.2 channels (Fig. 9 D).

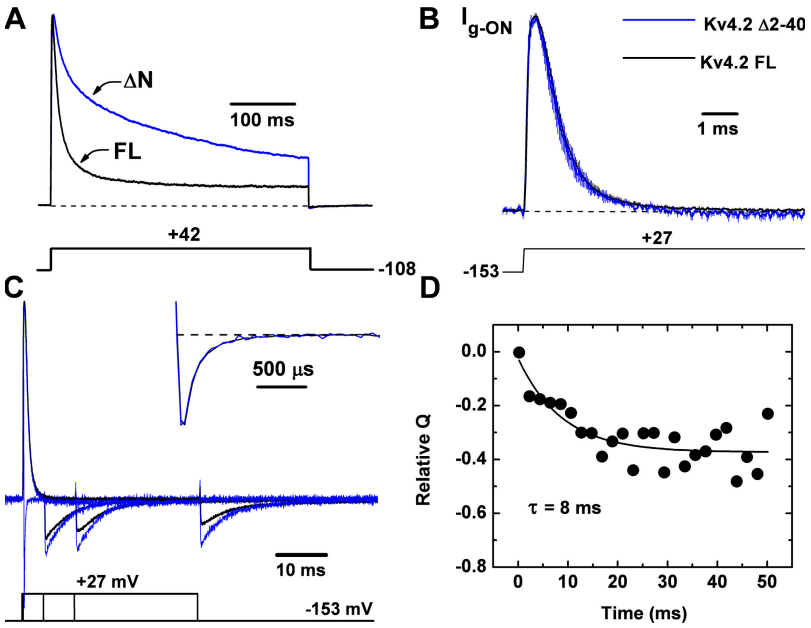

Figure 10. The Kv4.2 N terminus slows Q_{OFF} at depolarized potentials. (A) Ionic currents were elicited by a voltage step from −108 mV to +42 mV for full-length Kv4.2 (FL, black line) and Δ2–40 Kv4.2 (ΔN, blue line) channels. (B) I_{gON} was elicited by a voltage step from −153 to +27 mV. Current traces represent the average of five (Kv4.2) and three (Δ2-40 Kv4.2) experiments and the vertical lines correspond to the standard errors. (C) Average I_gs were normalized to the I_{gON} to compare the I_{gOFF}s measured by hyperpolarizations to −153 mV after depolarizations of increasing duration to +27 mV. To determine the contribution of the N terminus to Q-immobilization in a curve-fitting independent manner, the relative Q difference was measured by integrating the area bounded by the two I_{gOFF} current traces from Kv4.2 and Δ2–40 Kv4.2 channels. Inset, overlay I_{gOFF}s after a 0.2-ms depolarization. (D) An exponential function with τ corresponding to the fast time constant of macroscopic inactivation of Kv4.2 channels (8 ms) adequately described the increase in the relative Q difference over time (solid line).

Q-immobilization at Hyperpolarized Potentials Is Independent of the N-terminal Inactivation Gate

The role of the Kv4.2 N terminus is a primary concern in interpreting the mechanism of Q-immobilization because, in the absence of KChIPs, Kv4 channels undergo open-state N-type–like inactivation (Gebauer et al., 2004). The interaction between N-type inactivation and Q-immobilization in Shaker-B Kv channels results from the slowing of deactivation (and Q return) induced by pore occlusion by the N-terminal inactivation gate (Bezanilla et al., 1991; Roux et al., 1998). Therefore, we investigated fast Q-immobilization in the full-length and N-terminal–deleted (Δ2–40) Kv4.2 channels. This deletion eliminates the Kv4.2 N-terminal inactivation gate and thereby slows inactivation substantially (Fig. 10 A) (Zhu et al., 1999), but has no effect on activation as determined from the lack of change in the ON gating current (I_{gON}, Fig. 10 B). To examine fast Q-immobilization, the OFF gating current (I_{gOFF}) was measured by hyperpolarizations to −153 mV following depolarizations to +27 mV (to populate the open state; Fig. 10 C). Progressively longer depolarizations resulted in a progressively slower relaxation of the I_{gOFF} from full-length Kv4.2 channels, indicating hindered deactivation (Fig. 10 C). To analyze these observations, the averaged I_gs from the full-length Kv4.2 and Δ2–40 Kv4.2 channels (from several cells, $n = 3$–5; Fig. 10, legend) were normalized relative to I_{gON} and overlaid. When the depolarization to +27 is very short (200 μs), the corresponding I_{gOFF} traces from Δ2–40 and the full-length Kv4.2 channels are identical (Fig. 10 C, inset); however, as the depolarization is prolonged, the I_{gOFF} changes significantly (Fig. 10 C). The I_{gOFF} from Δ2–40 Kv4.2 channels had a more prominent fast component, which eventually crossed over the slower control I_{gOFF} from the full-length Kv4.2 counterpart. The change in the area under the two current traces (between the onset of the hyperpolarization and the crossover point) was taken as an indicator of the relative change in gating charge kinetics due to the N-terminal deletion (Fig. 10, legend); and consequently, the time dependence of this parameter is a measurement of fast N-terminal–dependent Q-immobilization, which was well described by assuming an exponential decay (τ = 8 ms) that accounted for ∼40% of the total Q. The time constant of this decay is almost identical to the time constant of fast inactivation (∼9 ms). Therefore, fast Q-immobilization in Kv4.2 channels expressed in the absence of KChIPs may correspond to an N-terminus–dependent open-state inactivation similar to that of Shaker-B Kv channels (Gebauer et al., 2004).

If the Kv4.2 N-terminal gate is capable of immobilizing Q from open states, it may play a role in slow Q-immobilization from closed states (Roux et al., 1998; Armstrong, 2006). We therefore investigated slow Q-immobilization in Δ2–40 Kv4.2 channels. Deletion of the N terminus resulted in modest changes in gating parameters and significant slowing of macroscopic inactivation (Fig. 10 A; Fig. 11 A; Table I). The time course and voltage dependence of slow Q-immobilization and remobilization were also unchanged by the Kv4.2 N-terminal deletion (Fig. 11, B and C). Therefore, although the N terminus plays a role in fast Q-immobilization at depolarized voltages, slow Q-immobilization from closed states at hyperpolarized voltages is independent of the Kv4.2 N-terminal inactivation gate.

An Expanded CSI Model Explains the Link between Slow Q-immobilization and Inactivation of Kv4.2 Channels

Kinetic schemes proposed by the Aldrich's, Bezanilla's, and Sigworth's groups have successfully modeled the

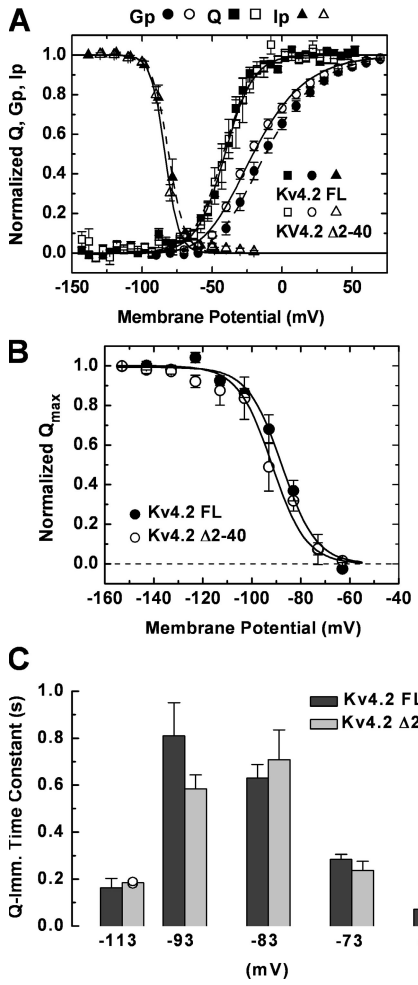

Figure 11. Steady-state Q-immobilization is independent of the Kv4.2 N terminus. (A) Gp-V (circles), $Q_{ON}V$ (squares), and I_{SS} (triangles) curves from Kv4.2 (black symbols) and Δ2–40 Kv4.2 (hollow symbols) channels were analyzed as described under Materials and methods (Data Analysis). The best-fit parameters were as follows: Gp-V $V_{1/2}$ = −13 mV (Kv4.2), −22.2 mV (Δ2–40 Kv4.2), k = 23.2 mV (Kv4.2), k = 23.2 mV (Δ2–40 Kv4.2); $Q_{ON}V$ $V_{1/2}$ = −42 mV (Kv4.2), −43 mV (Δ2–40 Kv4.2), z = 2.4 e_0 (Kv4.2), z = 2.4 e_0 (Δ2–40 Kv4.2); I_{SS} $V_{1/2}$ = −81 mV (Kv4.2), −84 mV (Δ2–40 Kv4.2), k = 5.7 mV (Kv4.2), 4.9 mV (Δ2–40 Kv4.2). (B) Q-availability curves from Kv4.2 (filled circles) and Δ2–40 Kv4.2 (hollow circles) channels were analyzed as described in Fig. 3 legend; and the best-fit parameters were as follows: $V_{1/2}$ (Kv4.2) = −88 mV and z (Kv4.2) = 3.6 e_0; $V_{1/2}$ (Δ2–40 Kv4.2) = −92 mV and z (Δ2–40 Kv4.2) = 3.6 e_0; n = 3–5 independent experiments. (C) Time constants of Q-immobilization for Kv4.2 and Δ2–40 Kv4.2 channels are represented as bars. Differences were not statistically significant ($P < 0.05$). Time constants from voltages with $n < 3$ are represented as individual data points.

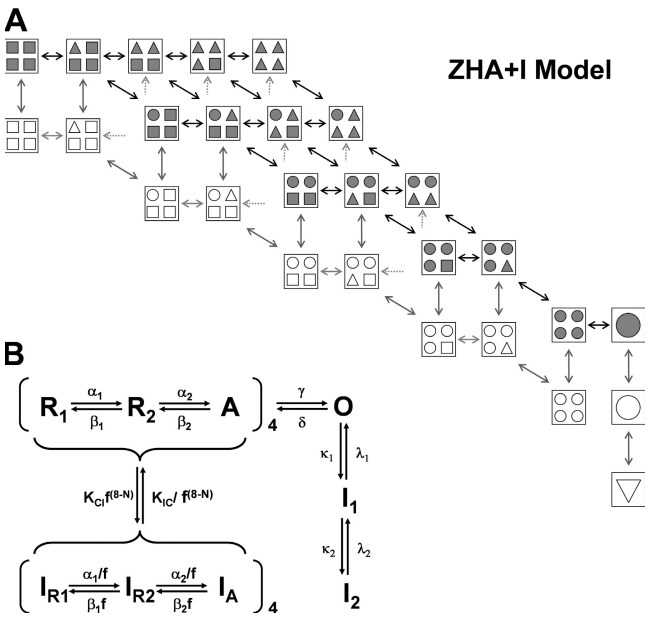

Figure 12. Kinetic scheme of Kv4.2 channel gating. This model is a modified version of the Zagotta-Hoshi-Aldrich model (ZHA plus inactivation = ZHA + I Model) shown in its full form (A) and an abbreviated form (B). Each voltage sensor undergoes two voltage-dependent conformational changes upon activation (R_1-R_2 and R_2-A transitions in B). The resting state (R1 in B) is represented by a square, the partially activated conformational (R_2 in B) is represented by a triangle (horizontal path in A, α_1 in B), and the fully activated conformation (A) is represented by a circle (diagonal path in A, α_2 in B). Inactivated states are represented by hollow symbols. All three voltage sensor conformations are inactivation permissive (vertical path in B), and transitions from closed (filled symbols) to closed-inactivated states (hollow symbols) are governed by an allosteric factor ($f^{(8-N)}$). The channel must undergo eight transitions (N indicates the degree of activation) among closed states between the resting state (four filled squares, N = 0) and the preopen closed state (four filled circles, N = 8). The rate of inactivation is therefore modified by the degree of activation (via the allosteric factor) so that it is most favorable from the preopen closed state (N = 8). For the sake of artistic representation, several closed-inactivated states have been excluded in A. Transitions to and from these states are represented by dotted arrows. Once all voltage sensors adopt the fully activated conformation, channels may enter the open state (single filled circle) from which open state inactivation may occur (single hollow symbols).

major features of Kv channel activation gating (Zagotta et al., 1994a; Schoppa and Sigworth, 1998; Bezanilla, 2000). Given its relative simplicity, we adopted the Zagotta-Hoshi-Aldrich (ZHA) scheme to develop a new CSI model for Kv4.2 channels (Fig. 12). Essentially, the modified ZHA model (ZHA + I model) includes two activation transitions per subunit of the tetrameric Kv channel and a single concerted opening step. To account for Q-immobilization, the ZHA + I model also includes coupled inactivation (Bähring et al., 2001a; Beck et al., 2002; Kaulin et al., 2007). Thus, it assumes that resting and activated subunits are inactivation permissive (Fig. 12 B) and the presence of a two-step open-state inactivation pathway. The magnitude of an "allosteric factor" (f) controls whether inactivation is more likely to occur from early or late closed states in the activation pathway.

To test whether the ZHA + I model can serve as a theoretical framework that helps explain the link between inactivation and slow Q-immobilization more quantitatively, we applied a global kinetic modeling approach

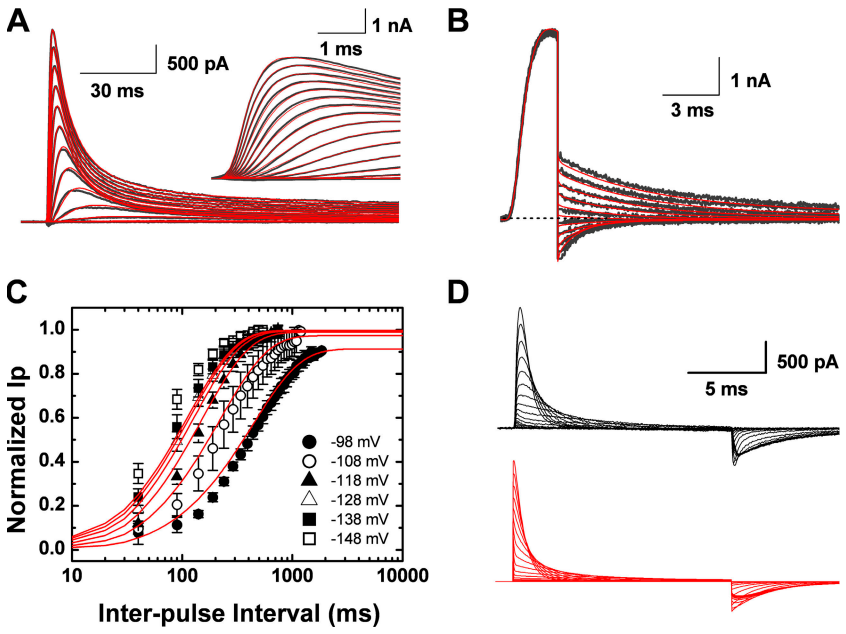

Figure 13. Global kinetic modeling of Kv4.2 channel gating. In all panels, experimental data (black) and global best-fits (red) are shown for comparison. (A) Experimental currents (average of five independent experiments) were elicited by step depolarizations from −100 to +50 mV in 10-mV increments from a holding potential of −100 mV. Inset, an expanded view of the activation phase of the currents (−100 to +100 mV in 10-mV increments from a holding potential of −100 mV). (B) Experimental tail currents (average of three independent experiments) were evoked by test pulses between −140 and −50 mV after a depolarization to +50 mV. (C) Recovery from inactivation curves at the indicated voltages replotted from Fig. 5 C. (D) Experimental family of gating currents elicited by step depolarizations from −143 to +47 mV in 10-mV increments from a holding potential of −153 mV (top; average of five independent determinations) and corresponding best fit (bottom).

(Materials and methods) that is experimentally constrained by all voltage- and time-dependent macroscopic properties of the ionic currents and the kinetics of I_{gON} and I_{gOFF} simultaneously (see limitations below). This model yielded an excellent best global fit for the kinetics and voltage dependence of activation, inactivation, and deactivation of the ionic currents, and described the corresponding I_gs and the $Q_{ON}V$ curve reasonably well (Fig. 13 and Fig. 14, B and C). The best global fit parameters predict prominent closed-state inactivation originating from the pre-open closed state, and a quasi-absorbing inactivated state (i.e., a very slow backward rate constant in the inactivation transitions; Table II), which is more favorably occupied upon membrane depolarization. Then, as a validation strategy, we used the best-fit parameters of the model to simulate the activation curves and the relationship between Q-immobilization and inactivation (Fig. 14). We found an excellent agreement between observed and simulated $Q_{ON}V$ and Gp-V (Fig, 14 A) curves. Importantly, the ZHA + I model predicted identical time constants of inactivation and Q-immobilization between −90 and −60 mV, and it accounted for the voltage dependence of the time constants of inactivation quite well (Fig. 14 C). Furthermore, we verified the stringent simultaneous measurements of inactivation and Q-immobilization kinetics by assuming the best-fit parameters from the ZHA + I model and plotting the outcome as shown in Fig. 8, B and D, and Fig. 9, B and D (Fig. 14 D). Clearly, this simulation produced the biphasic decay of Q and the exact correlation between inactivation the development of Q-immobilization. Therefore, Q-immobilization and inactivation in Kv4.2 channels can be seen as equivalent manifestations (in terms of kinetics and voltage dependence) of the same process; conceivably, the conformational change underlying Q-immobilization renders the channels reluctant to open (i.e., closed-state inactivated).

Limitations of the Global Kinetic Modeling and the ZHA + I Model

The best global fit produced an excellent description of all time- and voltage-dependent properties of the ionic currents (Fig. 13 and Fig. 14, B–D), and also predicted the Gp-V and $Q_{ON}V$ curves accurately (Fig. 14 A). However, the overall kinetics of the observed gating currents was slower than that of the best-fit gating currents (Fig. 13 D). This outcome was not surprising because the I_g measurements required special experimental conditions (pore blocked by CTX, internal Cs^+, and no internal K^+) that could account for the discrepancy. A slight effect of CTX is apparent when comparing the $1 - Q_{ON}V$ relations in Fig. 8 C, but Cs^+ appeared to have no active effect (relative to nonpermeant NMG^+) on the $Q_{ON}V$ relation and the development of Q-immobilization (see Fig. S1, available at http://www.jgp.org/cgi/content/full/jgp.200709938/DC1). Also, given these experimental limitations, the observed I_{gON} and I_{gOFF} were the only information included in the global dataset to account for Q kinetics semi-quantitatively (Fig. 13 D), and therefore, the global fit was inherently biased toward ionic current measurements. Assuming the ZHA + I model, a global fit of the family of I_gs over a broad range of membrane potentials (unconstrained by the ionic current measurements) yielded an improved description of the observed Q kinetics (see Fig. S4). However, some discrepancies remained (e.g., I_{gOFF}). Similar disagreements concerning I_{gOFF} were acknowledged in the study of Shaker-B channels by Zagotta et al. (1994a). Therefore, the two-step activation of the voltage sensor in the ZHA model (Fig. 12 B) may not be sufficient to account for

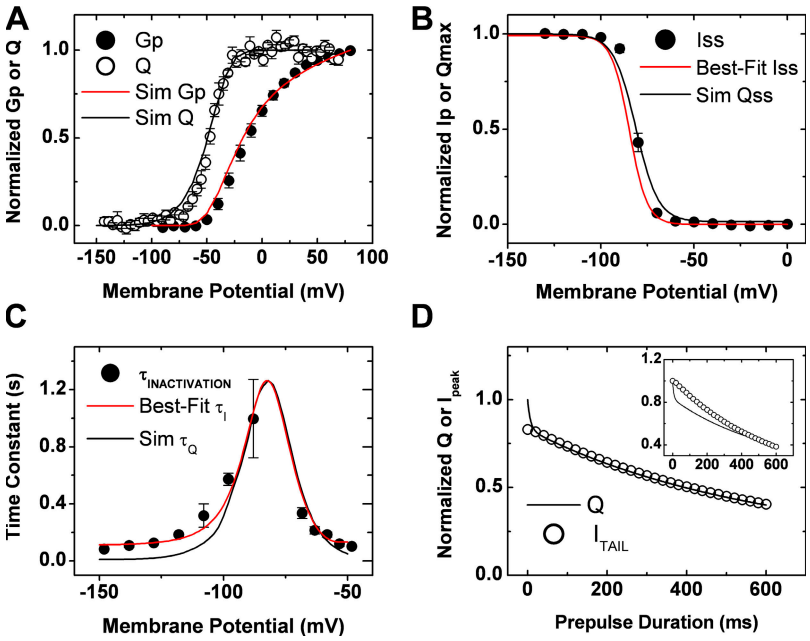

Figure 14. The ZHA + I model predicts equivalent kinetics and voltage dependence of inactivation and Q-immobilization. (A) The global best fit of the ZHA + I model ($Q_{ON}V$ curve, black line; Gp-V curve, red line) accurately simulates the experimental $Q_{ON}V$ (hollow circles) and Gp-V relations (filled circles). (B) Best-fit and experimental I_{SS} (red line and filled circles, respectively) curves. The simulated Q-availability curve (Sim Q_{SS}) is shown for comparison (black line). (C) The ZHA + I model accurately describes (best fit, red line) the voltage dependence of the time constants of inactivation (experimental data, filled circles). The simulated time constants of Q-immobilization (Sim τ_Q) are shown for comparison (black line). (D) Simulation of simultaneous inactivation (hollow circles) and Q-immobilization (black line) at −70 mV. Curves are renormalized as explained previously (Figs. 8 and 9). Inset, Q decay is biphasic (see text).

the detailed complexity of the Kv4.2 gating current and the underlying activation process. More complex activation schemes (Schoppa and Sigworth, 1998) were not considered in the global fit strategy because they add several more adjustable parameters to an expanded model with inactivation; and given the experimental limitations, it was not considered a fruitful approach.

The Kinetic Basis of Slow Q-immobilization in Kv4.2 Channels

Given that Q is conserved (i.e., the number of functional channels is constant) (Fig. 4 B, legend), how can the proposed model explain the reversible apparent Q-loss (Fig. 6)? Essentially, this phenomenon occurs because the Q can move along two energetically distinct but interconnected pathways (Fig. 12 A). In one pathway, the Q moves among activated states, and in the other, the Q moves among inactivated states. When the Q moves in the latter pathway channels cannot open. Whether and how the Q moves in one pathway or the other is dictated by the "allosteric factor" *f*, which is an indicator of the energetic coupling between the two pathways and the relative stabilities of the inactivated states. If $f < 1$, the forward (α) and backward (β) rate constants in the

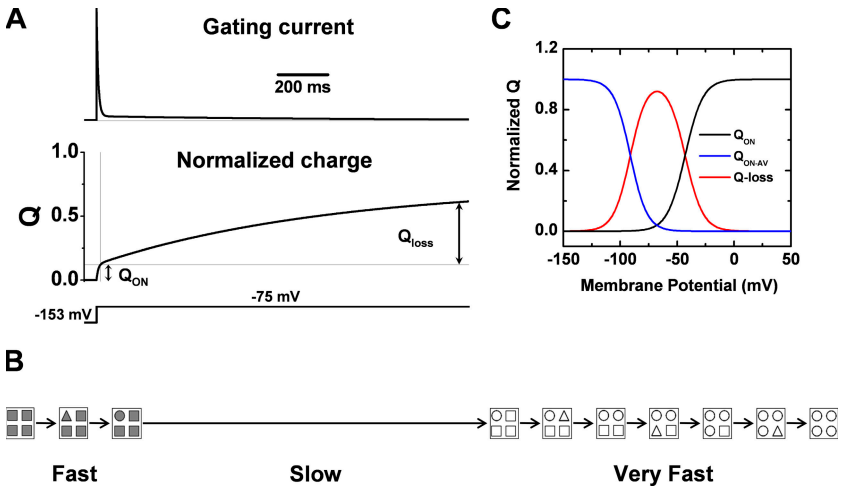

Figure 15. The kinetic basis of the apparent Q loss in Kv4.2 channels. (A and B) A step depolarization to −75 mV allows channels to populate closed states proximal to the resting state, which is associated with the rapid movement of a small fraction of Q (Q_{ON}). These partially activated channels slowly inactivate. Even though subsequent transitions among the closed-inactivated states occur rapidly and involve the same Q that moves among the noninactivated counterparts, no gating current is detected under experimental conditions because the rate-limiting inactivation transitions are unsynchronized and slow (Fig. S3). The slow phase of gating charge movement is clearly apparent in the simulation. Experimentally, however, the undetected slow charge movement contributes to an apparent Q loss. (C) The relationship between $Q_{ON}V$, $Q_{ON}V$-available, and the apparent Q loss. The lines representing $Q_{ON}V$ and $Q_{ON}V$-available are the corresponding best fits shown in Fig. 14, A and B, respectively; and Q loss is calculated as the difference between 1 − $Q_{ON}V$ and $Q_{ON}V$-available (see Fig. 2).

TABLE II

Best-Fit Parameters of the ZHA + I Model[a]

	Rate constant ($V = 0$)	z
	s^{-1}	e_0
α_1	1091.8	0.29
β_1	3299.5	−1.23
α_2	5971.1	0.1
β_2	21.1	−0.59
γ	9303.5	0.09
δ	2054.1	−0.11
κ_1	103.9	0
λ_1	43.6	0
κ_2	29.5	0
λ_2	33.3	0
k_{CI}	180.5	0
k_{IC}	0.009	0

The rate constants that control the voltage-dependent transitions (α_1, β_1,α_2, β_2, γ, δ) are assumed to depend exponentially on membrane potential according to the relationships $x(V) = x_0\exp(z_X eV/kT)$, where z_x, is the corresponding equivalent electronic charges, e is the electronic charge, V is the membrane potential, k is Boltzmann constant, and T is the absolute temperature. The total gating charge per channel is 9 e_0. The allosteric factor f is 0.42.

[a]ZHA + I model as depicted in Fig. 12.

inactivation pathway are accelerated and retarded, respectively (Fig. 12 B). Thus, relative to the speed of Q movement along the activation pathway, forward charge-carrying transitions are faster along the inactivation pathway. This relation would seem paradoxical when trying to account for the apparent Q-immobilization.

Fig. 15 explains the basis of the apparent Q-loss or immobilization. Assuming the best-fit parameters in the ZHA + I model (Table II), we simulated a 1500-ms depolarizing step from −153 to −75 mV, which elicits an I_g that relaxes in two distinct phases (fast and very slow) (Fig. 15 A). The Q that moves during the fast spike phase is associated with initial activation and represents ~10% of the total Q (Fig. 15 B). This relatively small fraction of Q moves within the first 10 ms of the pulse and is readily observed in our experiments. The very slow phase of the I_g spans most the time and carries ~50% of the total Q (Fig. 15 B). Because this slow Q movement spreads over a relatively long time, it is not detectable in our measurements; that is, it appears to be lost in the fluctuations of the current. The slow relaxation of the Q is, however, important because it is associated with the slow rate-limiting transition of the channels from the activated pathway to the inactivated pathway; and once the channels are in the inactivated pathway there is rapid equilibration among Q-carrying state transitions as the channels enter the quasi-absorbing inactivated state at the end of this pathway. The bottom of Fig. 15 B illustrates an approximation of the correspondence between the most significant state transitions, the relaxation of the I_g, and the trajectory of Q movement. One can then see more clearly that the channels inactivate from early closed states at −75 mV. A single channel simulation clarifies this conclusion further (see Fig. S3). It is also significant that the maximal apparent Q loss occurs at −75 mV (Fig. 15 C); and that at hyperpolarized voltages (less than −75 mV) there is preferential inactivation from early closed states, whereas inactivation occurs preferentially from intermediate and late closed states (i.e., closer to the open state) at depolarized voltages (greater than −75 mV). Therefore, the minimal overlap between the experimental $Q_{ON}V$ and the Q available (Fig. 2) is a reliable indicator of preferential closed-state inactivation in Kv4.2 channels (Fig. 15 C).

DISCUSSION

We investigated the relationship between slow voltage-dependent Q-immobilization and closed-state inactivation in Kv4.2 channels. All observations and kinetic modeling converged to suggest that the two processes are fundamentally equivalent. Therefore, they can be seen as separate manifestations of a slow rearrangement of the channel's voltage sensor, which causes desensitization to voltage and renders the channel's activation gate reluctant to open. We will discuss the relationship of our study to previous investigations of Q-immobilization in other voltage-gated ion channels, and the mechanistic implications in terms of a reinterpretation of inactivation mechanisms in Kv4 channels and their possible impact on physiological processes.

Relation to Previous Studies

Pioneering studies by Armstrong and Bezanilla discovered the interaction between inactivation and the Q movements in voltage-gated Na^+ channels (Nav channels), and coined the term "gating charge immobilization" to describe how inactivation influences Q movement (Armstrong and Bezanilla, 1977). Since then, several studies have discovered and characterized similar phenomena in native and recombinant Nav, Kv, and Cav channels, and special emphasis has been placed on understanding Q-immobilization at the molecular level in Shaker-B Kv channels (Nonner, 1980; Bezanilla et al., 1991; Olcese et al., 1997; Roux et al., 1998; Jones et al., 1999; Sheets et al., 2000). In these channels, fast and slow Q-immobilizations are related to generally accepted molecular mechanisms of open-state inactivation. Occlusion of the inner mouth of the Shaker Kv channel pore in a fast N-type mechanism immobilizes 3/4 of the Q_{OFF} until the N-terminal gate dissociates and the activation gate closes (Bezanilla et al., 1991; Roux et al., 1998). In the slow P/C-type mechanism, slow Q-immobilization is associated with the stabilization of a localized pore collapse at the channel's outer mouth (Loots and Isacoff, 1998; Larsson and Elinder, 2000). This conformation of the voltage sensor is observed as a leftward-shifted QV curve, first reported in squid Nav channels (Armstrong and

Bezanilla, 1977; Bezanilla et al., 1982) and later investigated in recombinant Shaker Kv channels (Olcese et al., 1997). The leftward-shifted QV curve suggested that the Q of inactivated channels at depolarized membrane potentials experiences an energy landscape where the "up" state of the voltage sensor is strongly favored relative to the resting conformation ("down" state) (Olcese et al., 1997; Bezanilla et al., 1982). Q-immobilization that correlates with inactivation is also observed in Cav2.2 channels that undergo preferential closed-state inactivation (Jones et al., 1999). In this case, however, the leftward shift of the QV curve is not observed because inactivation occurs from a partially activated state only and Q undergoes no movement among inactivated channels over the voltage range where the channels undergo voltage-dependent activation (Jones et al., 1999).

A hyperpolarizing shift of the QV curve may be observed in certain Kv channels under conditions that do not induce significant inactivation but progressively favor the open state of the channel because the opening equilibrium is weakly voltage dependent (Wang et al., 2007b). In this case too, the voltage sensor is stabilized in its "up" state relative to the resting state. Analogously, Ca^{2+}-activated Kv channels exhibit distinct QV curves in the absence and presence of intracellular Ca^{2+}, which is also consistent with Q movement along two energetically distinct pathways (Horrigan and Aldrich, 1999, 2002).

Olcese et al. (1997) proposed that slow Q-immobilization in Shaker-B Kv channels corresponds to C-type inactivation. Namely, they argued that the pore mutant used in their study (W434F) undergoes slow Q-immobilization in spite of being permanently P-type inactivated. This argument led them to conclude that the P-type and C-type components represent two separable conformational changes underlying slow inactivation in Shaker-B Kv channels. Our observations are similar to those of Olcese et al., however, Kv4.2 channels exhibit profound Q-immobilization associated with steady-state inactivation that occurs at hyperpolarized voltages. Furthermore, we observed slow Q-immobilization when the pore of Kv4.2 channels was directly occluded by CTX, which binds inside the selectivity filter at an external site (Yu et al., 2005), and therefore, an external pore collapse is not likely to occur. In any case, it is clear that slow Q-immobilization can occur independently of a pore collapse in both Shaker-B and Kv4.2 channels. The underlying conformational change of the voltage sensors may thus correspond to C-type inactivation in both channels. However, while Shaker-B Kv channels undergo slow inactivation by coupling Q-immobilization to a pore collapse (P/C-type inactivation) (Loots and Isacoff, 1998), Kv4.2 channels lack stable P-type inactivation (Kaulin et al., 2007). Thus, C-type inactivation in Kv4.2 channels is coupled to an unidentified conformational change that prevents conduction or opening of the channel.

Reinterpretation of Inactivation Mechanisms in Kv4 Channels

In general, CSI is accepted as a plausible gating pathway in voltage-gated ion channels (Aldrich and Stevens, 1983; Aldrich et al., 1983; Goldman, 1995; Ayer and Sigworth, 1997; Olcese et al., 1997; Klemic et al., 1998; Jones et al., 1999; Bähring et al., 2001a; Beck et al., 2002; Claydon et al., 2007). However, the mechanism and molecular basis of CSI are not understood. The classical inactivation mechanisms could contribute to CSI in Kv channels if one assumes that (a) the N-terminal inactivation gate (N-type inactivation) can "pre-inactivate" the closed channel (Zhou et al., 2001; Armstrong, 2006), or (b) the pore collapses (P/C-type inactivation) before the main activation opens (Panyi and Deutsch, 2006). Alternatively, desensitization to voltage has been more recently proposed as the CSI mechanism in HCN channels (Shin et al., 2004), but it may also apply to Kv channels (Jerng et al., 2004). The later is a possible mechanism of CSI in Kv4 channels because slow and profound Q-immobilization at hyperpolarized voltages is independent of the Kv4 N-terminal inactivation gate (Fig. 11), and a P/C-type mechanism may not inactivate Kv4 channels (Kaulin et al., 2007). Thus, in light of the results reported here, one must ask the following: what mechanism is ultimately responsible for the relatively rapid and complete inactivation of Kv4.2 channels? What is the molecular link between Q-immobilization and inactivation of conductance?

Parting from the general similarity between our observations and those from Olcese et al., we propose that the voltage sensors of Shaker-B and Kv4 channels undergo fundamentally similar conformational changes when Q is immobilized (i.e., C-type inactivation). Although the exact mechanism of slow Q-immobilization is not known, it is clear from the leftward-shifted QV curve of inactivated channels (Fig. 4) that a sustained membrane depolarization changes the energy landscape of the voltage sensor. The key difference between Shaker-B and Kv4 channels lies in the way Q-immobilization impacts the pore domain. Conceivably, as the voltage sensor of Kv4 channels slowly immobilizes, it adopts a stable conformation that renders the internal activation gate reluctant to open, in other words, desensitized to voltage before it has a chance to open (i.e., closed-state inactivated). Otherwise, a strong but transient electromechanical coupling between the voltage sensor and the main activation is presumably responsible for the cooperative opening of the pore (Long et al., 2005, 2007; Pathak et al., 2007).

Voltage Sensor Movements Regulate I_{SA} Availability

The relationship between Q-immobilization and CSI suggests that the functional availability of Kv4 channels is directly controlled by the voltage sensors. Canonical models of Kv channel activation associate sudden changes

in membrane potential with rapid movements of the voltage sensors, which are ultimately responsible for fast voltage-dependent activation. The job of the voltage sensors, however, does not end with this task. Q-immobilization studies of voltage-gated ion channels have shown conclusively that sustained membrane depolarizations induce slower rearrangements of the voltage sensors before they reach a stable conformation (see above). In Kv4 channels, these slower conformational changes may be directly responsible for the installment of CSI, the process that regulates the functional availability of the K^+ currents that they mediate. Kv4 channels underlie I_{SA} in neurons (Birnbaum et al., 2004; Jerng et al., 2004); whether or not I_{SA} influences membrane excitability and thereby a variety of integrative processes (Hoffman et al., 1997; Cai et al., 2004; Kim et al., 2005, 2007) will depend on whether the voltage sensors have remobilized by hyperpolarization, and therefore, recovered from CSI. Kv4-specfic auxiliary subunits (KChIPs and DPLPs) that are integral parts of the native Kv4 channel complex may remodel the immobilization–remobilization cycle and CSI (Beck et al., 2002; Nadal et al., 2003; Jerng et al., 2004; Dougherty and Covarrubias, 2006).

We thank Drs. Richard Horn and Toshinori Hoshi for critical and insightful comments. Also, we thank the Covarrubias laboratory for support and fruitful discussions.

The work was supported by a research grant from the National Institutes of Health (R01 NS032337-13 to M. Covarrubias) and a Research Enhancement Award from Thomas Jefferson University (M. Covarrubias). K. Dougherty was supported by a training grant from National Institutes of Health (T32 AA007463-22).

Edward N. Pugh Jr. served as editor.

Submitted: 6 December 2007
Accepted: 4 February 2008

REFERENCES

Aldrich, R.W., D.P. Corey, and C.F. Stevens. 1983. A reinterpretation of mammalian sodium channel gating based on single channel recording. *Nature.* 306:436–441.

Aldrich, R.W., and C.F. Stevens. 1983. Inactivation of open and closed sodium channels determined separately. *Cold Spring Harb. Symp. Quant. Biol.* 48:147–153.

An, W.F., M.R. Bowlby, M. Betty, J. Cao, H.P. Ling, G. Mendoza, J.W. Hinson, K.I. Mattsson, B.W. Strassle, J.S. Trimmer, and K.J. Rhodes. 2000. Modulation of A-type potassium channels by a family of calcium sensors. *Nature.* 403:553–556.

Armstrong, C.M. 2006. Na channel inactivation from open and closed states. *Proc. Natl. Acad. Sci. USA.* 103:17991–17996.

Armstrong, C.M., and F. Bezanilla. 1977. Inactivation of the sodium channel. II. Gating current experiments. *J. Gen. Physiol.* 70:567–590.

Ayer, R.K.J., and F.J. Sigworth. 1997. Enhanced closed-state inactivation in a mutant Shaker K^+ channel. *J. Membr. Biol.* 157:215–230.

Bähring, R., L.M. Boland, A. Varghese, M. Gebauer, and O. Pongs. 2001a. Kinetic analysis of open- and closed-state inactivation transitions in human Kv4.2 A-type potassium channels. *J. Physiol.* 535:65–81.

Bähring, R., J. Dannenberg, H.C. Peters, T. Leicher, O. Pongs, and D. Isbrandt. 2001b. Conserved Kv4 N-terminal domain critical for effects of Kv channel-interacting protein 2.2 on channel expression and gating. *J. Biol. Chem.* 276:23888–23894.

Beck, E.J., M. Bowlby, W.F. An, K.J. Rhodes, and M. Covarrubias. 2002. Remodelling inactivation gating of Kv4 channels by KChIP-1, a small-molecular-weight calcium binding protein. *J. Physiol.* 538:691–706.

Beck, E.J., and M. Covarrubias. 2001. Kv4 channels exhibit modulation of closed-state inactivation in inside-out patches. *Biophys. J.* 81:867–883.

Bezanilla, F. 2000. The voltage sensor in voltage-dependent ion channels. *Physiol. Rev.* 80:555–592.

Bezanilla, F., E. Perozo, D.M. Papazian, and E. Stefani. 1991. Molecular basis of gating charge immobilization in Shaker potassium channels. *Science.* 254:679–683.

Bezanilla, F., R.E. Taylor, and J.M. Fernandez. 1982. Distribution and kinetics of membrane dielectric polarization. 1. Long-term inactivation of gating currents. *J. Gen. Physiol.* 79:21–40.

Birnbaum, S.G., A.W. Varga, L.L. Yuan, A.E. Anderson, J.D. Sweatt, and L.A. Schrader. 2004. Structure and function of Kv4-family transient potassium channels. *Physiol. Rev.* 84:803–833.

Cai, X., C.W. Liang, S. Muralidharan, J.P. Kao, C.M. Tang, and S.M. Thompson. 2004. Unique roles of SK and Kv4.2 potassium channels in dendritic integration. *Neuron.* 44:351–364.

Claydon, T.W., M. Vaid, S. Rezazadeh, D.C. Kwan, S.J. Kehl, and D. Fedida. 2007. A direct demonstration of closed-state inactivation of K^+ channels at low pH. *J. Gen. Physiol.* 129:437–455.

Cordero-Morales, J.F., V. Jogini, A. Lewis, V. Vasquez, D.M. Cortes, B. Roux, and E. Perozo. 2007. Molecular driving forces determining potassium channel slow inactivation. *Nat. Struct. Mol. Biol.* 14:1062–1069.

Dougherty, K., and M. Covarrubias. 2006. A dipeptidyl aminopeptidase-like protein remodels gating charge dynamics in Kv4.2 channels. *J. Gen. Physiol.* 128:745–753.

Fedida, D., R. Bouchard, and F.S. Chen. 1996. Slow gating charge immobilization in the human potassium channel Kv1.5 and its prevention by 4-aminopyridine. *J. Physiol.* 494:377–387.

Gebauer, M., D. Isbrandt, K. Sauter, B. Callsen, A. Nolting, O. Pongs, and R. Bähring. 2004. N-type inactivation features of Kv4.2 channel gating. *Biophys. J.* 86:210–223.

Goldman, L. 1995. Sodium channel inactivation from closed states: evidence for an intrinsic voltage dependency. *Biophys. J.* 69:2369–2377.

Hoffman, D.A., J.C. Magee, C.M. Colbert, and D. Johnston. 1997. K^+ channel regulation of signal propagation in dendrites of hippocampal pyramidal neurons. *Nature.* 387:869–875.

Horrigan, F.T., and R.W. Aldrich. 1999. Allosteric voltage gating of potassium channels II. Mslo channel gating charge movement in the absence of Ca^{2+}. *J. Gen. Physiol.* 114:305–336.

Horrigan, F.T., and R.W. Aldrich. 2002. Coupling between voltage sensor activation, Ca^{2+} binding and channel opening in large conductance (BK) potassium channels. *J. Gen. Physiol.* 120:267–305.

Jerng, H.H., P.J. Pfaffinger, and M. Covarrubias. 2004. Molecular physiology and modulation of somatodendritic A-type potassium channels. *Mol. Cell. Neurosci.* 27:343–369.

Jones, L.P., C.D. DeMaria, and D.T. Yue. 1999. N-type calcium channel inactivation probed by gating-current analysis. *Biophys. J.* 76:2530–2552.

Jurman, M.E., L.M. Boland, Y. Liu, and G. Yellen. 1994. Visual identification of individual transfected cells for electrophysiology using antibody-coated beads. *Biotechniques.* 17:876–881.

Kaulin, Y., J. De Santiago-Castillo, C. Rocha, and M. Covarrubias. 2007. Mechanism of the modulation of Kv4:KChIP-1 by external K^+. *Biophys. J.* 94:1241–1251.

Kim, J., D.S. Wei, and D.A. Hoffman. 2005. Kv4 potassium channel subunits control action potential repolarization and frequency dependent broadening in hippocampal CA1 pyramidal neurons. *J. Physiol.* 569:41–57.

Kim, J., S.C. Jung, A.M. Clemens, R.S. Petralia, and D.A. Hoffman. 2007. Regulation of dendritic excitability by activity-dependent trafficking of the A-type K^+ channel subunit Kv4.2 in hippocarnpal neurons. *Neuron.* 54:933–947.

Kim, L.A., J. Furst, M.H. Butler, S. Xu, N. Grigorieff, and S.A. Goldstein. 2004. Ito channels are octomeric complexes with four subunits of each Kv4.2 and K^+ channel-interacting protein 2. *J. Biol. Chem.* 279:5549–5554.

Klemic, K.G., C.C. Shieh, G.E. Kirsch, and S.W. Jones. 1998. Inactivation of Kv2.1 potassium channels. *Biophys. J.* 74:1779–1789.

Larsson, H.P., and F. Elinder. 2000. A conserved glutamate is important for slow inactivation in K^+ channels. *Neuron.* 27:573–583.

Long, S.B., E.B. Campbell, and R. MacKinnon. 2005. Voltage sensor of Kv1.2: structural basis of electromechanical coupling. *Science.* 309:903–908.

Long, S.B., X. Tao, E.B. Campbell, and R. MacKinnon. 2007. Atomic structure of a voltage-dependent K^+ channel in a lipid membrane-like environment. *Nature.* 450:376–382.

Loots, E., and E.Y. Isacoff. 1998. Protein rearrangements underlying slow inactivation of the Shaker K^+ channel. *J. Gen. Physiol.* 112:377–389.

Nadal, M.S., A. Ozaita, Y. Amarillo, E. V. de Miera, Y. Ma, W. Mo, E.M. Goldberg, Y. Misumi, Y. Ikehara, T.A. Neubert, and B. Rudy. 2003. The CD26-related dipeptidyl aminopeptidase-like protein DPPX is a critical component of neuronal A-type K^+ channels. *Neuron.* 37:449–461.

Nonner, W. 1980. Relations between the inactivation of sodium channels and the immobilization of gating charge in frog myelinated nerve. *J. Physiol.* 299:573–603.

O'Leary, M.E., and R. Horn. 1994. Internal block of human heart sodium channels by symmetrical tetra-alkylammoniums. *J. Gen. Physiol.* 104:507–522.

Olcese, R., R. Latorre, L. Toro, F. Bezanilla, and E. Stefani. 1997. Correlation between charge movement and ionic current during slow inactivation in Shaker K^+ channels. *J. Gen. Physiol.* 110:579–589.

Olcese, R., D. Sigg, R. Latorre, F. Bezanilla, and E. Stefani. 2001. A conducting state with properties of a slow inactivated state in a shaker K^+ channel mutant. *J. Gen. Physiol.* 117:149–163.

Panyi, G., and C. Deutsch. 2006. Cross talk between activation and slow inactivation gates of Shaker potassium channels. *J. Gen. Physiol.* 128:547–559.

Pathak, M.M., V. Yarov-Yarovoy, G. Agarwal, B. Roux, P. Barth, S. Kohout, F. Tombola, and E.Y. Isacoff. 2007. Closing in on the resting state of the shaker K^+ channel. *Neuron.* 56:124–140.

Pioletti, M., F. Findeisen, G.L. Hura, and D.L. Minor Jr. 2006. Three-dimensional structure of the KChIP1-Kv4.3 T1 complex reveals a cross-shaped octamer. *Nat. Struct. Mol. Biol.* 13:987–995.

Roux, M.J., R. Olcese, L. Toro, F. Bezanilla, and E. Stefani. 1998. Fast inactivation in Shaker K^+ channels. Properties of ionic and gating currents. *J. Gen. Physiol.* 111:625–638.

Ruben, P.C., J.G. Starkus, and M.D. Rayner. 1992. Steady-state availability of sodium channels. Interactions between activation and slow inactivation. *Biophys. J.* 61:941–955.

Schoppa, N.E., and F.J. Sigworth. 1998. Activation of Shaker potassium channels. III. An activation gating model for wild-type and V2 mutant channels. *J. Gen. Physiol.* 111:313–342.

Serodio, P., C. Kentros, and B. Rudy. 1994. Identification of molecular components of A-type channels activating at subthreshold potentials. *J. Neurophysiol.* 72:1516–1529.

Sheets, M.F., J.W. Kyle, and D.A. Hanck. 2000. The role of the putative inactivation lid in sodium channel gating current immobilization. *J. Gen. Physiol.* 115:609–620.

Shin, K.S., C. Maertens, C. Proenza, B.S. Rothberg, and G. Yellen. 2004. Inactivation in HCN channels results from reclosure of the activation gate: desensitization to voltage. *Neuron.* 41:737–744.

Wang, H., Y. Yan, Q. Liu, Y. Huang, Y. Shen, L. Chen, Y. Chen, Q. Yang, Q. Hao, K. Wang, and J. Chai. 2007a. Structural basis for modulation of Kv4 K^+ channels by auxiliary KChIP subunits. *Nat. Neurosci.* 10:32–39.

Wang, Z., B. Robertson, and D. Fedida. 2007b. Gating currents from a Kv3 subfamily potassium channel: charge movement and modification by BDS-II toxin. *J. Physiol.* 584:755–767.

Yellen, G., D. Sodickson, T.Y. Chen, and M.E. Jurman. 1994. An engineered cysteine in the external mouth of a K^+ channel allows inactivation to be modulated by metal binding. *Biophys. J.* 66:1068–1075.

Yu, L., C. Sun, D. Song, J. Shen, N. Xu, A. Gunasekera, P.J. Hajduk, and E.T. Olejniczak. 2005. Nuclear magnetic resonance structural studies of a potassium channel-charybdotoxin complex. *Biochemistry.* 44:15834–15841.

Zagotta, W.N., T. Hoshi, and R.W. Aldrich. 1994a. Shaker potassium channel gating. III: Evaluation of kinetic models for activation. *J. Gen. Physiol.* 103:321–362.

Zagotta, W.N., T. Hoshi, J. Dittman, and R.W. Aldrich. 1994b. Shaker potassium channel gating. II: Transitions in the activation pathway. *J. Gen. Physiol.* 103:279–319.

Zhou, M., J.H. Morais-Cabral, S. Mann, and R. MacKinnon. 2001. Potassium channel receptor site for the inactivation gate and quaternary amine inhibitors. *Nature.* 411:657–661.

Zhu, X.R., A. Wulf, M. Schwarz, D. Isbrandt, and O. Pongs. 1999. Characterization of human Kv4.2 mediating a rapidly-inactivating transient voltage-sensitive K^+ current. *Receptors Channels.* 6:387–400.